Struct Chem (2006) 17:105–120
DOI 10.1007/s11224-006-9005-5

ORIGINAL PAPER

Mössbauer, vibrational spectroscopic and solution X-ray diffraction studies of the structure of iron(III) complexes formed with indole-3-alkanoic acids in acidic aqueous solutions

Krisztina Kovács · Alexander A. Kamnev · János Mink · Csaba Németh · Ernő Kuzmann · Tünde Megyes · Tamás Grósz · Hedvig Medzihradszky-Schweiger · Attila Vértes

Received: 6 October 2005 / Accepted: 7 December 2005 / Published online: 25 April 2006

Abstract The chemical reactions between iron(III) and indole-3-acetic (IAA), -propionic (IPA), and -butyric (IBA) acids were studied in acidic aqueous solutions. The motivation of this work was that IAA is one of the most powerful natural plant-growth-regulating substances (phytohormones of the auxin series). Mössbauer spectra of the frozen aqueous solutions of iron(III) with indole-3-alkanoic acids as ligands (L), showed parallel reactions between Fe^{3+} and the ligands. Partly, it resulted in a complex formation which precipitated in aqueous solution and partly, in a redox process with iron(II) and the oxidised indole-3-alkanoic acids as products. The Mössbauer parameters of the Fe^{2+} species suggested a hexaaquo coordination environment. The chemical composition and coordination structure of the precipitated complexes were investigated using elemental analysis, Mössbauer spectroscopy, Fourier transform infrared (FTIR) and Raman spectroscopic techniques. The complexes were soluble in some organic solvents. So, Mössbauer, FTIR and solution X-ray diffraction measurements were carried out on the solution of complexes in acetone, hexadeutero acetone and methanol, respectively. The data obtained supported the existence of the μ-dihydroxo-bridging structure of the dimer: $[L_2Fe<(OH)_2>FeL_2]$ (where L is indole-3-propionate, -acetate or -butyrate).

Keywords Indole-3-alkanoic acids · Iron(III) complexes · Moessbauer spectroscopy · Fourier transform infrared (FTIR) spectroscopy · Fourier transform Raman spectroscopy · Solution X-ray diffraction · Structure elucidation

K. Kovács · E. Kuzmann · A. Vértes
Research Group for Nuclear Techniques in Structural Chemistry, Hungarian Academy of Sciences; Department of Nuclear Chemistry, Eötvös Loránd University, 1518, Budapest 112, Hungary
email: vertesa@ludens.elte.hu

A. A. Kamnev (✉)
Laboratory of Biochemistry of Plant-Bacterial Symbioses, Institute of Biochemistry and Physiology of Plants and Microorganisms, Russian Academy of Sciences, 410049 Saratov, Russia
e-mail: aakamnev@ibppm.sgu.ru

J. Mink · C. Németh · T. Megyes · T. Grósz
Chemical Research Center of the Hungarian Academy of Sciences, 1525, Budapest, P.O. Box 77, Hungary

J. Mink
Analytical Chemistry Research Group, Hungarian Academy of Sciences and Faculty of International Technology, Research Institute of Chemical and Process Engineering, University of Veszprém, Veszprém, 8200, Hungary

H. Medzihradszky-Schweiger
Research Group of Peptide Chemistry, Department of Organic Chemistry, Eötvös Loránd University, 1518, Budapest 112, Hungary

Introduction

Indole-3-acetic acid (IAA) is one of the most powerful natural plant-growth-regulating substances (phytohormones of the auxin series) that are capable of stimulating cell division and promoting cell elongation [1–3]. It is well documented to be synthesized also by many soil microorganisms, in particular, in the rhizosphere where it plays an essential role in plant–microbe interactions [4, 5]. The excretion of auxins directly into the soil, along with their phytoregulating effects, can lead to chemical interactions involving

metal ions. Among these, iron(III) is an essential microelement ubiquitous in various soils. Our earlier studies have shown [6–10] the possibility of redox processes involving ferric ions as well as IAA or some other chemically and/or metabolically related naturally occurring substances, such as indole-3-propionic (IPA), indole-3-butyric (IBA), anthranilic acids and tryptophan, in slightly acidic aqueous solutions. This could be of ecological significance, since Fe^{3+} has a poor biological availability over a wide pH range owing to its full hydrolysis and extremely low solubility of ferric (oxy)hydroxides, but it can be reductively solubilised under appropriate conditions (in slightly acidic media) giving a more bioavailable iron(II). It was also shown [11] that in circumneutral aqueous media, the presence of IAA or tryptophan in solution influences the phase composition of ferric oxyhydroxides that crystallise from the amorphous material.

On the other hand, studying the mode of coordination of indolic compounds to iron(III) can provide additional information helpful in understanding the enzymatic degradation of auxins. The formation of a triple complex (peroxidase–IAA–oxygen) has been proposed for the oxidative degradation mechanism of IAA including as a key step a simple one-electron transfer from the IAA molecule to the ferric moiety of the peroxidase heme [12]. In earlier papers [13, 14], an attempt was made to consider the aqueous Fe^{3+}–IAA system as an inorganic model for the peroxidase–IAA complex. Ferric chloride and IAA-containing aqueous solutions were studied in detail [14], but the structure of the precipitate obtained was not characterised.

In the present work, chemical interaction of iron(III) nitrate with IAA, IPA, IBA in aqueous solutions was monitored and, in particular, the structure of the solid complexes formed was investigated in detail, including comparative studies of deuterated materials and measurements in nonaqueous (acetone, methanol) solutions. The coordination properties of the isolated solid materials were studied using ^{57}Fe Mössbauer, Fourier transform infrared (FTIR), FT-Raman spectroscopic techniques, solution X-ray diffraction and elemental analysis.

Experimental

The materials for Mössbauer measurements in aqueous solutions were prepared using iron(III) solutions containing enriched (ca. 90% ^{57}Fe) iron dissolved in nitric acid at elevated temperature. The stock solution was diluted down to 0.01 M concentration with regard to iron(III), with pH 0.9. The indole derivatives used (IAA, IPA, IBA) were dissolved in water adding KOH to the water solutions up to pH 6–7. The concentration of the ligands was 0.03 M. Addition of iron(III) nitrate to IAA, IPA or IBA in solution (up to the 1:3 metal-to-acid molar ratio) resulted in the colour change of the solutions and the formation of cocoa-brown precipitates indicating complexation of Fe^{3+} with the indole-3-alkanoic acids. The final pH values of the mixtures were 2.0–2.5 (measured using an OP-211 laboratory pX/mV meter, Radelkis, Hungary). The precipitates were filtered out after 15 min, dried on the filter paper at room temperature for a few days and placed in a cryostat cooled with liquid nitrogen. The Mössbauer spectra of the filtered rapidly frozen solutions were also recorded.

To study the structure and possible structural changes of the complexes by dissolving them in an organic solvent, e.g. in acetone, and adding a small amount of water to the solutions, ca. 0.1 M samples (with regard to total Fe) were measured using the rapid-freezing (quenching) method [15]. For these experiments, as well as for the FTIR, FT-Raman measurements and for elemental analysis, the solid complexes were synthesized using natural (not enriched with ^{57}Fe) iron(III) nitrate, the conditions being the same as described above. The precipitates were filtered out, washed three times with distilled water and dried in air.

All Mössbauer spectra were recorded at liquid nitrogen temperature (ca. 80 K) using a conventional constant-acceleration type Mössbauer spectrometer with a "cold-finger" cryostat filled with liquid nitrogen. A ^{57}Co(Rh) source was used, and the spectrometer was calibrated with α-Fe at room temperature, which is the reference for all isomer shifts reported in this paper. Statistical treatment of the Mössbauer spectra was performed with the assumption of Lorentzian lineshapes in order to calculate isomer shifts (δ, mm/s), quadrupole splittings (Δ, mm/s), line widths (full width at half maximum, Γ, mm/s) and partial resonant absorption areas (S_r,%) for all spectral components [16].

The elemental analyses were carried out using Vario EL III (Elementar Analysensystem Gmbh) and the Fe content was measured as Fe_2O_3.

Mid-IR (200–4000 cm^{-1}, resolution 4 cm^{-1}, 128 scans) absorption spectra were recorded in purged nitrogen atmosphere using a Bio-Rad (Digilab) FTS-175 spectrometer with a CsI beamsplitter. Far-infrared spectra (50–700 cm^{-1}, resolution 4 cm^{-1}) were recorded with a Bio-Rad (Digilab) FTS-40 spectrometer with a wire-mesh beamsplitter. Pellets were prepared of the solid samples, diluted with caesium iodide for mid-IR and with polyethylene for far-IR. FT-Raman spectra of liquid samples (dissolved complexes) were recorded using a dedicated Bio-Rad FT-Raman spectrometer with an Adlas DTY-321 Nd-YAG-laser (1024 nm, 150 mW). However, in order to avoid laser-induced decomposition of the solid samples, the latter were studied using a Renishaw System 1000 spectrometer equipped with a Leica DMLM microscope, a diode laser (782 nm, 20 mW) and a Peltier-cooled CCD detector. Deuterated samples were obtained by exposing the solids to D_2O vapour for several days; their FTIR spectra were compared to those of the respective solids similarly

treated with H_2O vapour. All measurements were performed at ambient temperature.

The solution X-ray diffraction studies were carried out using 0.5 mol dm^{-3} solution of the Fe–IAA complex in methanol (density, $\rho = 1$ g cm^{-3}, linear X-ray absorption coefficient $\mu = 1.7371$ cm^{-1}, atomic number density $\rho_0 = 0.1058$ $Å^{-3}$); methanol was used as a solvent in order to simplify calculations. Measurements were performed at ambient temperature (24 ± 1°C), with a Θ-Θ goniometer of symmetrical transmission geometry using MoK_α radiation (wavelength $\lambda = 0.7107$ Å) with a graphite monochromator placed in the diffracted beam. The liquid sample holder had plane-parallel windows prepared from 6.3-μm thick mylar foils. The scattering angle range of the measurement spanned over $1.28° \leq 2\Theta \leq 120°$ corresponding to a range of $0.2\ Å^{-1} \leq k \leq 15.3\ Å^{-1}$ of the scattering variable $k = (4\pi/\lambda)\cdot\sin\Theta$. Over 100,000 counts were collected at each of 150 discrete angles selected with steps $k \approx 0.1\ Å^{-1}$, in several repeated runs (10,000 counts at each point).

The measurement technique and data treatment were essentially the same as described previously [17]. The measured intensities were corrected for background, polarisation, absorption and Compton scattering [18]. The Compton contribution was evaluated by a semi-empirical method in order to account for the monochromator discrimination [19]. The Compton intensities that were necessary for the corrections were calculated using analytical formulae [20, 21]. The experimental structure function is defined as

$$h(k) = \frac{I(k) - \sum_\alpha x_\alpha f_\alpha^2(k)}{M(k)}, \qquad (1)$$

where $I(k)$ is the corrected coherent intensity of the scattered beam normalised to electron units [22]; $f_\alpha(k)$ and x_α are the scattering amplitude and mole fraction for an α-type particle, respectively; $M(k)$ is the modification function, $M(k) = \{[\Sigma x_\alpha f_\alpha(k)]^2\}\exp(-0.01k^2)$. The coherent scattering amplitudes of the ions and the methanol molecule were computed according to analytical formulae suggested by Hajdu [20] and Cromer and Waber [23]. The methanol molecules were treated in the atomic representation. The necessary parameters were taken from the International Tables for X-ray Crystallography [24].

The experimental pair correlation function was computed from the structure function $h(k)$ by Fourier transformation according to

$$g(r) = 1 + \frac{1}{2\pi^2 r\rho_0}\int_{k_{\min}}^{k_{\max}} \frac{kh(k)\sin(kr)dk}{M(k)}, \qquad (2)$$

where r is the interatomic distance, $k_{\min}$ and $k_{\max}$ are the lower and upper limits of the experimental data, ρ_0 is the bulk number density of the stoichiometric units. After repeated Fourier transformations, when the non-physical peaks present in the $g(r)$ at small r values were removed, the structure function was corrected for residual systematic errors [19].

Results and discussion

Mössbauer measurements

A Mössbauer spectrum of the frozen aqueous solution of iron(III) nitrate (0.01 M) is presented in Fig. 1a. The pronounced line broadening is a sign of magnetic relaxation due to a slow paramagnetic spin relaxation. Namely, the spin–spin and spin–lattice interactions are weak because of the low concentration of Fe^{3+} and the relatively low temperature (80 K), respectively. (At the temperature of 4.5 K, the Mössbauer spectrum of the same solution shows a magnetic splitting [25].)

Mössbauer spectra of the frozen aqueous solutions of iron(III) with indole-3-alkanoic acids, filtered 15 min and 2 days after mixing and rapidly frozen, are shown in Fig. 1b–g. The parameters of the spectra given in Table 1 suggest the existence of parallel reactions between Fe^{3+} and the ligands (L):

$$Fe^{3+} + L \rightarrow \begin{cases} \text{Fe(III) complex (precipitate)} \\ Fe^{2+} + \text{oxidised L} \end{cases}$$

The Mössbauer parameters of the resulting Fe^{2+} species (isomer shifts $\delta = 1.39 \pm 0.01$ mm/s and quadrupole splittings $\Delta = 3.35 \pm 0.03$ mm/s) show that it has a hexaaquo coordination environment [25]. Comparing the spectral intensities (cf. Fig. 1b–d and e–g) it can be seen that both after 15 min and after 2 days of contact of the indolic acids with iron(III), in IAA solutions there appears significantly more ferrous iron (represented by the above-mentioned doublet with larger δ and Δ values) than in the Fe–IPA or Fe–IBA systems, indicating a stronger reducing capability of IAA towards iron(III) in this series of indole-3-alkanoic acids, evidently related to the ease of the IAA side-chain decarboxylation [12–14]. The other two components of the spectra (see Fig. 1b–g, except Fig. 1e) represent the iron(III) complexes with the corresponding ligands (doublet with $\delta = 0.52$ to 0.55 mm/s; see Table 1) and the remaining unreacted Fe^{3+} ions (broad single line).

The results of elemental analysis of the poorly soluble Fe–IAA, Fe–IPA, Fe–IBA complexes are given in Table 2. The supposed composition of the Fe–IAA/IPA most closely corresponds to that of the μ-$(OH)_2$-bridged complex $[L_2Fe{<}(OH)_2{>}FeL_2]$ (where L is the deprotonated IAA or IPA moiety). The same result was suggested for the Fe–IBA complex earlier [10], and now it is confirmed for all the three complexes obtained using detailed FTIR and

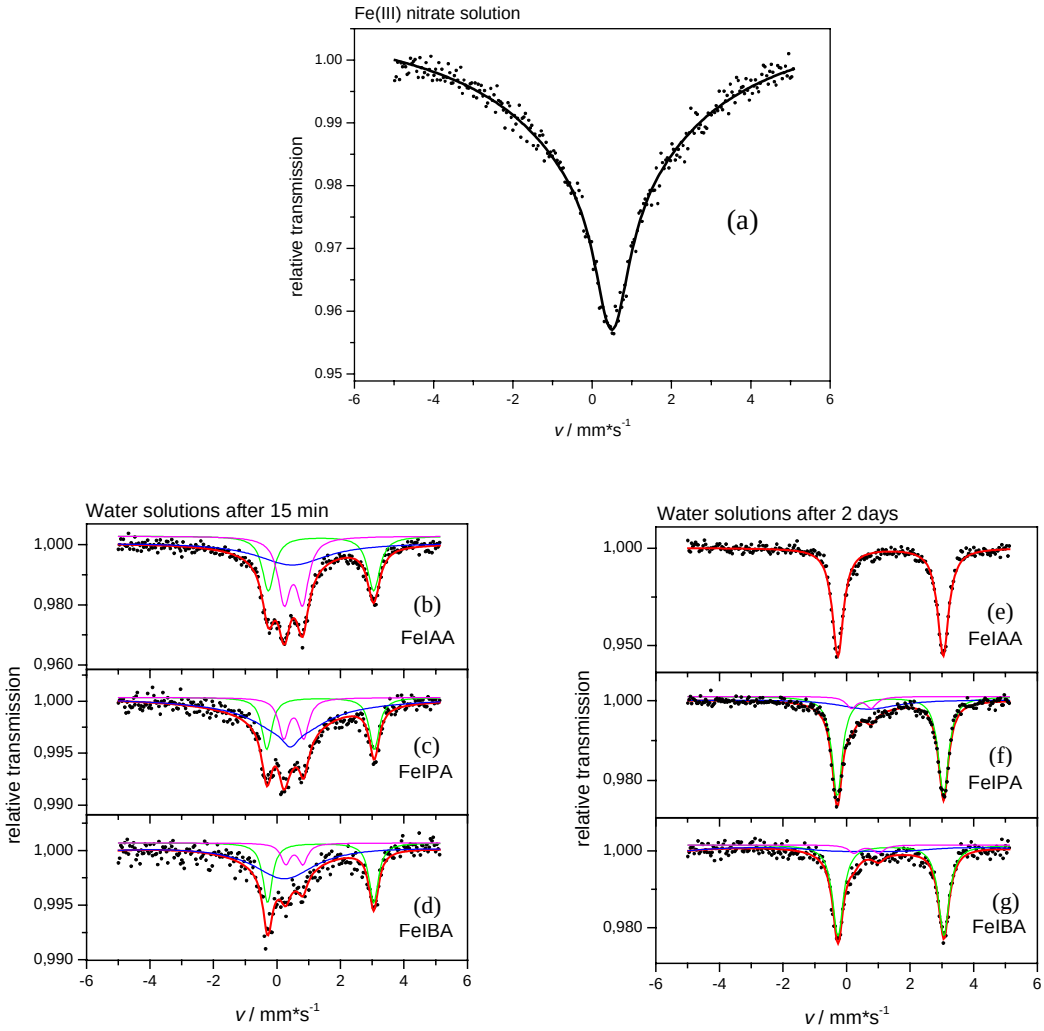

Fig. 1 Mössbauer spectra of 0.01 M ^{57}Fe nitrate (*a*), mixed ^{57}Fe nitrate and indole-3-alkanoic acid aqueous solutions filtered 15 min (b–d) and 2 days (*e–g*) after mixing (pH ≈ 2 to 2.5; measured at $T = 80$ K). (b), (e) indole-3-acetic acid; (*c*), (*f*) indole-3-propionic acid; (*d*), (*g*) indole-3-butyric acid

Table 1 Mössbauer parameters[a] for aqueous ^{57}Fe(III) nitrate-containing solutions of indole-3-alkanoic acids (pH = 2.0 to 2.5) filtered and rapidly frozen 15 min and 2 days after mixing (see Fig. 1b–g)

System	Spectral component	δ [b] (mm/s)	Δ[c] (mm/s)	Γ[d] (mm/s)	S_r[e] (%) (after 15 min)	S_r[e] (%) (after 2 days)
Fe–IAA	Doublet I	0.52(2)	0.58(3)	0.47(6)	12.8	–
	Doublet II	1.40(2)	3.32(4)	0.47(6)	11.3	100.0
Fe–IPA	Doublet I	0.53(4)	0.63(9)	0.38(7)	22.4	9.9
	Doublet II	1.38(2)	3.38(5)	0.38(7)	24.0	59.5
Fe–IBA	Doublet I	0.55(8)	0.50(10)	0.36(8)	8.2	4.5
	Doublet II	1.38(3)	3.34(5)	0.36(8)	16.1	50.8

All samples measured at $T = 80$ K. In all cases (except Fe–IAA, 2 days after mixing; see Fig. 1e), the third, relaxed component (not given in this Table) was fitted with $\delta = 0.42$ mm/s as a fixed value (the other parameters of this component could not be obtained due to the insufficient range of the velocity applied).

[a]Errors (in the last digits) are given in parentheses (3σ).

[b]Isomer shift.

[c]Quadrupole splitting.

[d]Full linewidth at half maximum.

[e]Partial resonant absorption areas of spectral components which represent relative contents of the corresponding iron forms assuming a common recoilless fraction for all components.

Table 2 Elemental analysis data (found, wt.%) as compared to those calculated for the dimer formulas of iron(III)–IAA, iron(III)–IPA and iron(III)–IBA complexes

Formula[a]	C	H	N	Fe
$[(IA)_2Fe\langle(OH)_2\rangle Fe(IA)_2]$	57,02	4.08	6.65	13.26
Found:	54.44	4.10	6.38	13.07
$[(IP)_2Fe\langle(OH)_2\rangle Fe(IP)_2]$	58.81	4.72	6.24	12.43
Found:	57.18	4.44	6.15	12.85
$[(IB)_2Fe\langle(OH)_2\rangle Fe(IB)_2]$	60.38	5.29	5.87	11.70
Found:	59.87	5.17	5.66	11.21

[a]IA, IP and IB represent indole-3-acetate ($C_{10}H_8NO_2^-$), indole-3-propionate ($C_{11}H_{10}NO_2^-$) and indole-3-butyrate ($C_{12}H_{12}NO_2^-$), respectively.

FT-Raman experiments as well (see below). It is worth mentioning that another series of measurements showed the possibility of mononuclear $Fe^{III}(IA)_3$ complex formation [8] (where IA is indole-3-acetate). This can be explained by the well-known experimental fact that even very small pH differences strongly affect the dimerisation of iron(III) species in aqueous solutions [25].

The solid complexes that were filtered out give an intensive symmetric quadrupole doublet with the parameters typical for high-spin Fe^{3+} (Fig. 2, Table 3) in distorted octahedral coordination. It is noticeable that the line widths observed are somewhat larger than could be expected for a well-defined structure. This suggests either a lack of a well-defined structure in the amorphous solids (proved by powder XRD measurements; not shown) or the existence of slightly different ligand spheres of Fe^{3+} that can be realised through some oligomeric species, besides the dimeric component, and the formation of some μ-$(OH)_2$-bridged $[Fe_2(H_2O)_4(OH)_2]^{4+}$ complexes [15]. This can also account for the observed differences from the calculated values in the elemental analysis results for IAA and IPA (see Table 2).

Each of the Mössbauer spectra of the complexes in acetone solutions shows one well-resolved quadrupole doublet as well (Fig. 3). The lack of a magnetic structure is an evidence that the iron(III) species have a dimeric structure with a fast spin–spin relaxation [25]. The doublets for the

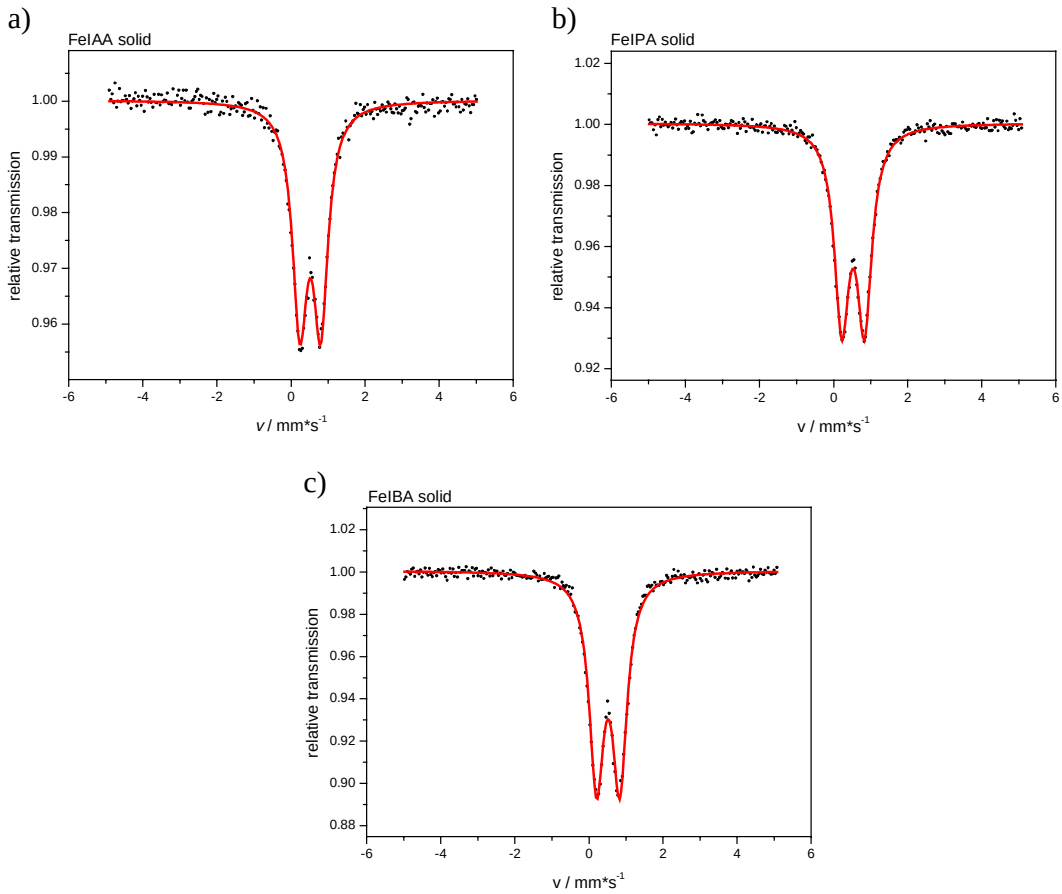

Fig. 2 Mössbauer spectra of the solid complexes: (a) Fe–IAA, (b) Fe–IPA, (c) Fe–IBA (measured at $T = 80$ K)

Table 3 Mössbauer parameters[a] for the solid samples filtered out from the aqueous solutions 15 min after mixing iron(III) nitrate solution with a solution of indole-3-acetic (IAA), -propionic (IPA) or -butyric (IBA) acids (measured at $T = 80$ K)

Complex	Spectral component	δ[b] (mm/s)	Δ[c] (mm/s)	Γ[d] (mm/s)	S_r[e] (%)
Fe–IAA	Fe^{3+}	0.517(2)	0.564(4)	0.489(7)	100.0
Fe–IPA	Fe^{3+}	0.519(1)	0.633(2)	0.487(4)	100.0
Fe–IBA	Fe^{3+}	0.527(2)	0.618(3)	0.488(5)	100.0

[a]Errors (in the last digits) are indicated in parentheses; the same for Table 4.

[b]Isomer shift (relative to α-Fe at room temperature).

[c]Quadrupole splitting.

[d]Full linewidth at half maximum.

[e]Partial resonant absorption areas of spectral components which represent relative contents of the corresponding iron form assuming a common recoilless fraction for all forms.

acetone solutions have the isomer shifts and quadrupole splittings (Table 4) very close to those for the solid materials (see Table 3), which indicates similar structures of the iron(III) microenvironment both in the solid state and in the acetone solutions. However, FTIR measurements showed some free COOH moieties appearing in all cases. This is a clear evidence for some structural changes in the complexes upon dissolving them in acetone that are not detectable by Mössbauer spectroscopy (see FTIR data below). These results suppose that already the traces of water impurity in the acetone used (which originally contains ca. 0.05% water) is capable of hydrolytically replacing the COO^- moiety, possibly giving free R–COOH ligands (where R–COOH represents indole-3-acetic, -propionic or -butyric acid). It is evident that after adding more water to the acetone solutions (0.02 cm^3 per 1 ml of acetone solution, which corresponds to ~ 10 H_2O molecules per 1 atom of Fe^{3+}), the structural changes become visible in Mössbauer spectra as well, with the quadrupole splittings increasing by 0.19, 0.16 and 0.13 mm/s for the Fe–IAA, Fe–IPA and Fe–IBA complexes, respectively (see Table 4; Fig. 4). The latter indicates the formation of a more asymmetric coordination of iron(III) upon adding water due to the aforementioned ligand exchange, which in this case evidently proceeds to a greater extent.

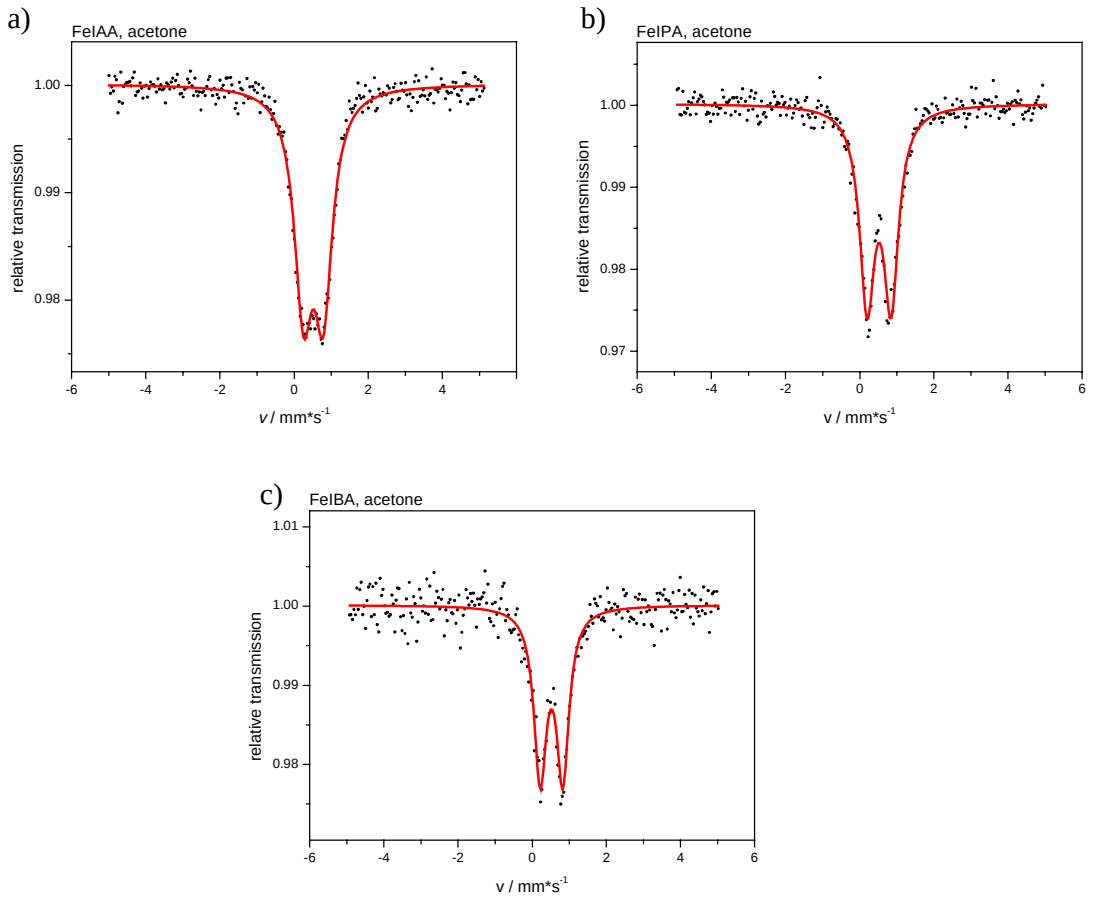

Fig. 3 Mössbauer spectra of 0.1 M acetone solutions of the complexes without adding water: (a) Fe–IAA, (b) Fe–IPA, (c) Fe–IBA (measured at $T = 80$ K)

FTIR and FT-Raman measurements

FTIR and Raman results confirm the above mentioned structural properties. The characteristic features of NH and COOH groups of the IAA, IPA and IBA ligands can be distinguished in FTIR and FT-Raman spectra (Fig. 5), as summarized in Table 5. The very broad band with a maximum absorption about 3000 cm^{-1} characteristic of carboxylic acids is due to the associated OH···O stretching vibration of their dimers (see Fig. 5A; this broad band is absent in the FT-Raman spectra in Fig. 5B). On the top of these bands, the C–H stretching features are superimposed. In all cases, there is a very strong and intensive typical band at about 1700 cm^{-1} characteristic of the C=O stretching vibrations of the carboxylic groups. The typical weak bands on the low-frequency wings (under 500 cm^{-1}; see Fig. 5A) are due to overtones and combinations of O–H and C–O stretches of the COOH groups.

The bands collected in Table 6 were selected as "new" bands in the spectra of the complexes, as compared to those of free acids. Broad and medium intensity absorption bands at about 3550 cm^{-1} were detected and assigned to stretching vibrations of the OH groups bound to Fe(III).

Due to the complex formation, the NH stretching bands are shifted only by 20–30 cm^{-1} in both directions (for Fe–IAA, at 3415 cm^{-1} (shifted up); for Fe–IPA, at 3415 cm^{-1} (down) and for Fe–IBA, at 3415 cm^{-1} (up)), showing rather a weak perturbation (see IPA and Fe–IPA spectra as an example in Fig. 6; other spectra not shown). The changes may be ascribed to the alterations of the system of H-bonds in the crystalline solid acids (involving both the COOH and, to some extent, N–H moieties) upon their coordination via the carboxylic groups. Thus, most probably the nitrogen of the indole moiety (with its lone electron pair strongly involved in the aromatic system including the pyrrole ring) does not contribute to the coordination of the IAA, IPA or IBA ligands with iron(III) in the complexes and, in particular, is not deprotonated upon complexation. The broad band about 3000 cm^{-1} and weak features around 2600 cm^{-1}, as well as the strong C=O stretching band at 1700 cm^{-1} characteristic of the carboxylic group (see Fig. 5A and Table 5) are totally absent in the FTIR spectra of the complexes. Instead, several new bands around 1580, 1525, 1430, 675, 625 and 550 cm^{-1} were recorded suggesting the presence of bidentate carboxylic groups, as can be seen from the proposed assignments in Table 6. The new bands assigned to wagging, twisting and rocking modes of CH_2 groups can be explained by conformational changes in the structure of IAA, IPA and IBA ligands when they become coordinated to the metal. The new C–C stretching bands of alkyl chains around 950 cm^{-1} can also be assigned to the conformational changes in the ligand structures occurring upon complexation.

Merely from the O–H stretching modes it is not possible to assign what type(s) of OH groups exist in the complexes. It is known that hydroxo complexes exhibit the M–OH bending mode around 1100 cm^{-1} and M–O stretching modes within the range 550–440 cm^{-1}. Since the vibrational spectra of these compounds are rather complex in the case of IPA and IBA, a deuteration experiment was performed. The Fe–IPA and Fe–IBA complexes had been exposed to D_2O vapour for several days, and the resulting FTIR spectra were compared in detail with FTIR spectra of the respective samples that had been similarly treated with H_2O vapour (in the latter case, their spectra were virtually identical to the original spectra of the complexes).

In line with our expectation, there are two types of exchangeable protons in the complexes: one type in the NH moiety, the other type being in the expected OH group. The spectrum of the deuterated Fe–IBA complex in the high-frequency range is presented in Fig. 7. The new bands can be clearly seen around 2500 cm^{-1}. The two spectra were subtracted from each other, and in the Fe–OH bending region the difference spectrum was obtained (Fig. 8), with the bands facing upward and characteristic of M–OD group and the bands appearing in the opposite direction referring to M–OH fragment(s). The two major features at 1093 and 912 cm^{-1} can be clearly assigned to FeOH and FeOD bending modes of bridging OH/OD groups, respectively. Note that there is lack of infrared spectroscopic data in the literature concerning hydroxy-bridged complexes of transition metals. For instance, a copper(II) bipyridyl complex was shown to exhibit a bridging OH bending mode at 955 cm^{-1}, which shifts to 710 cm^{-1} upon deuteration [26]. These reported bands are in agreement with our experimental observations.

The so-called deuterium-sensitive NH and OH group vibrations are listed in Table 7. Besides the above discussed, a Fe_2OH bridged moiety should exhibit isotope effects of the Fe–O stretching, Fe_2OH out-of-plane bending and Fe–O–Fe deformation modes. The strongest frequency shift was observed for the band at 480 cm^{-1} which moved to 473 cm^{-1} upon deuteration (Fig. 9). This band can be assigned to one of the Fe–O stretching modes of the Fe_2OH moiety. Note, for example, that some oxalate and bipyridyl complexes of Fe(III), Cr(III) and Co(III), containing bridging OH groups, exhibit vibrational bands around 500–540, 550–570 and 550–580 cm^{-1} for Fe(III), Cr(III) and Co(III), respectively [26]. The other two couples of bands marked in Fig. 9 at 582/578 and 281/278 cm^{-1} can be attributed to the out-of-plane bending mode of Fe_2OH/Fe_2OD and the deformational mode of Fe–O–Fe moieties, respectively.

One of the most important features in vibrational spectroscopic characterisation of metal complexes is the observation and assignment of metal–ligand stretching modes. As was described above, the stretching modes of the bridging OH group can be assigned on the basis of adequate frequency shifts due to deuteration (see Table 7). As for the carboxyls, generally the metal–oxygen stretching bands of

Table 4 Mössbauer parameters for the complexes of iron(III) with IAA, IPA and IBA dissolved in acetone (0.1 M relative to total Fe^{3+})

Complex	Spectral component	δ[a] (mm/s)	Δ[b] (mm/s)	Γ[c] (mm/s)	S_r[d] (%)
(a) No water added					
Fe–IAA	Fe^{3+}	0.517(4)	0.538(7)	0.60(1)	100.0
Fe–IPA	Fe^{3+}	0.528(4)	0.659(7)	0.51(1)	100.0
Fe–IBA	Fe^{3+}	0.527(7)	0.62(1)	0.43(2)	100.0
(b) Water added (2 v/v%)					
Fe–IAA	Fe^{3+}	0.498(8)	0.73(1)	0.65(2)	100.0
Fe–IPA	Fe^{3+}	0.520(6)	0.82(1)	0.54(1)	100.0
Fe–IBA	Fe^{3+}	0.512(8)	0.75(1)	0.52(2)	100.0

All measurements were performed at $T = 80$ K for solutions rapidly frozen in liquid nitrogen.

[a]Isomer shift (relative to α-Fe at room temperature).

[b]Quadrupole splitting.

[c]Full-line-width at half maximum.

[d]Partial resonant absorption areas of spectral components which represent relative contents of the corresponding iron form assuming a common recoilless fraction for all forms.

bidentate carboxylate groups are expected to show up in the far-infrared region, commonly within a spectral range of 600–300 cm^{-1}. For Fe–IBA, the new features (see the dashed bands in Fig. 10) obtained in this region are bands at 385, 347 and 324 cm^{-1} which are the best candidates for Fe–O stretches of the carboxylic ligands. A single Raman band was observed for Fe–IBA complex at 340 cm^{-1} (see Table 6). The low-frequency bands (below 300 cm^{-1}) can be assigned presumably to skeletal deformation modes of the complex. The same spectral range is shown for Fe–IPA in Fig. 11.

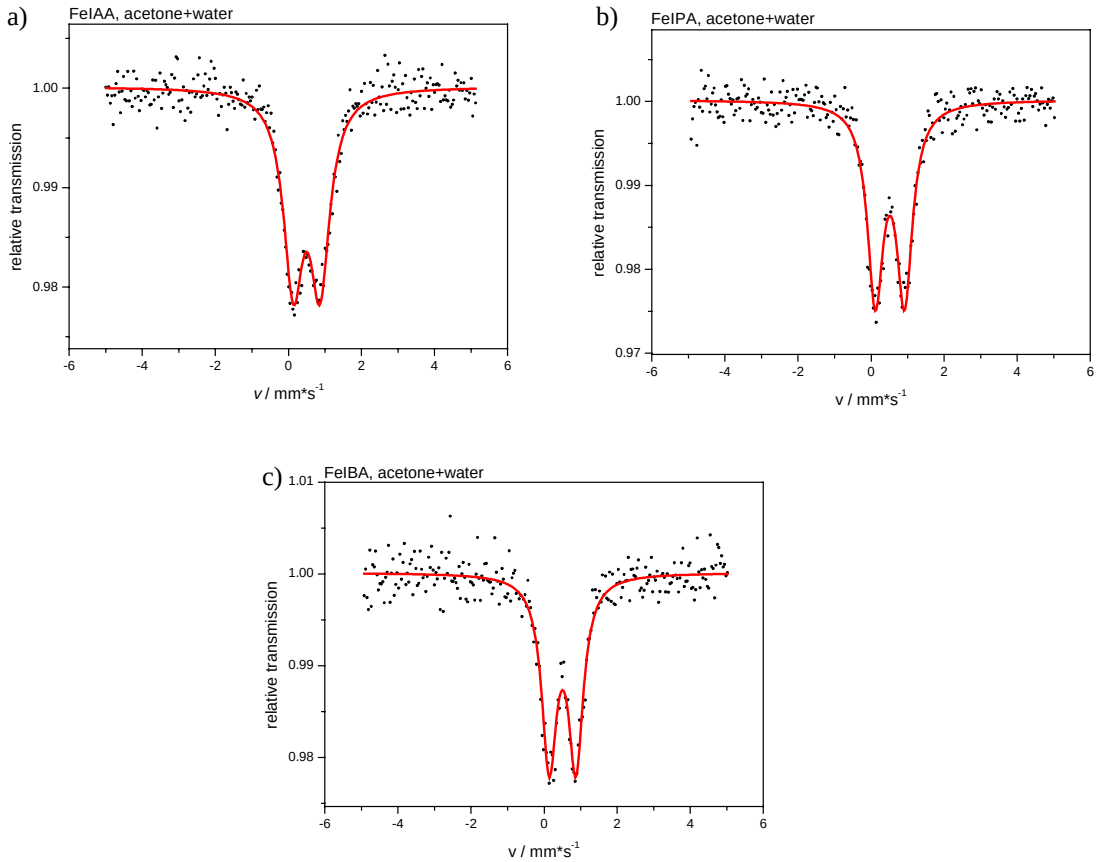

Fig. 4 Mössbauer spectra of 0.1 M acetone solutions of the complexes after adding 2 v/v% water to the samples: (a) Fe–IAA, (b) Fe–IPA, (c) Fe–IBA (measured at $T = 80$ K)

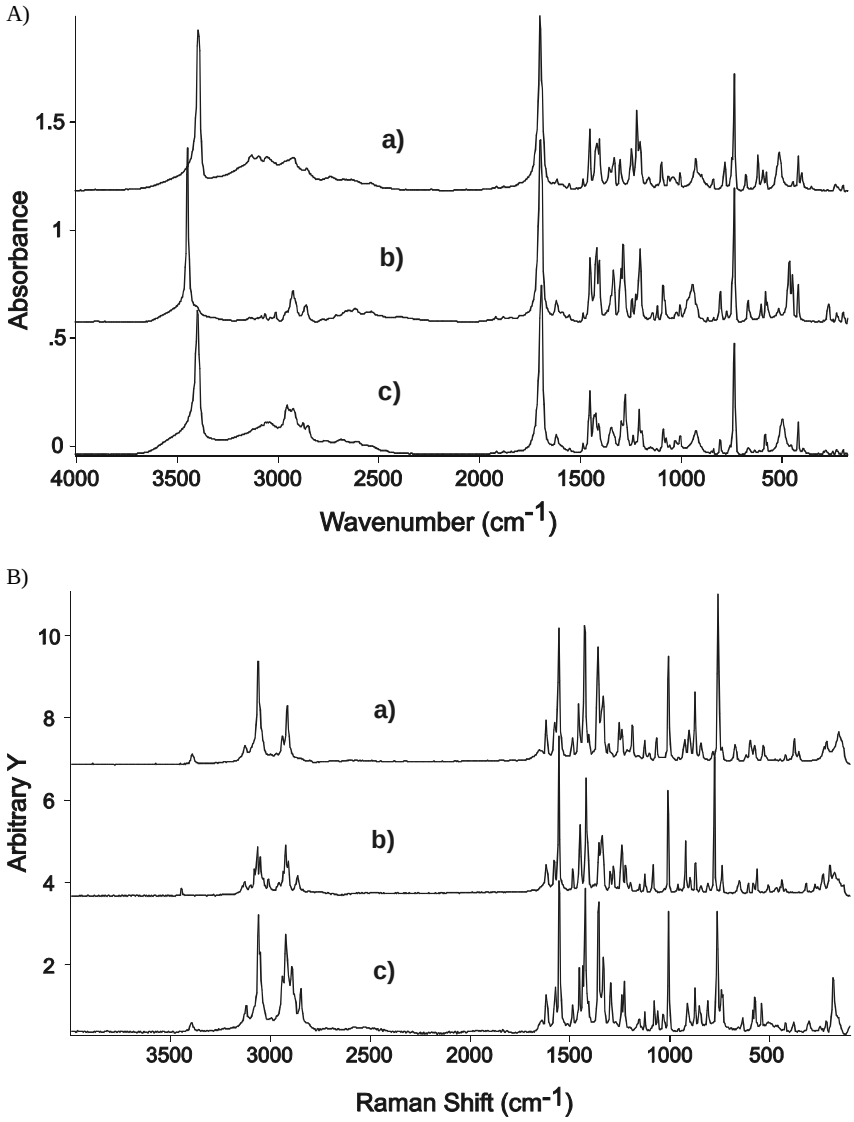

Fig. 5 Infrared (A) and Raman spectra (B) of indole-3-acetic acid (a), indole-3-propionic acid (b) and indole-3-butyric acid (c) in the spectral range 4000–200 cm^{-1}

Table 5 NH stretching and – COOH group frequencies[a] (cm^{-1}) obtained in the Fourier transform infrared and Raman spectra of solid indole-3-acetic (IAA), -propionic (IPA) and -butyric (IBA) acids

IAA		IPA		IBA		
IR	Raman	IR	Raman	IR	Raman	Assignments
3390 vs	3387 vw	3444 vs	3441 vw	3395 vs	3393 vw	NH stretch
2736 w,b	–	2655 w,b	–	2689 w,b	–	Overtones and combinations of OH deformations and C–O stretches of –COOH group
2636 vw,b	–	2616 vw,b	–	2632 vw,b	–	
2539 w,b	–	2535 vw,b	–	2544 vw	–	
1700 vs	–	1700 vs	–	1696 vs	–	C=O stretch
1305 m	1306 vw	1289 s	1283 m	1280 m	–	C–O stretch
1208 m	–	1208 m	–	1210 m	–	OH in plane bend
–	904 w	–	921 m	–	930 m,b	OH out of plane bend
684 w	674 w	672 w	665 w	672 w	–	C=O in plane def
601 w	–	–	–	–	–	COO waging
518 w,b	–	469 m	470 vw	502 m,b	500 vw	COO rocking

[a]Band notations: b, broad; s, strong; vs, very strong; m, medium; w, weak; vw, very weak.

Table 6 Selected infrared and Raman frequencies[a] (cm^{-1}) of the complexes different from the free ligand bands

FeIAA		FeIPA		FeIBA		
IR	Raman	IR	Raman	IR	Raman	Assignments
≈3530 mb		≈3550 m,b		3560 m,b		OH stretch
3415 s		3415s,b		3415 s		NH stretch
1590 vs	1597 vw	1586 vs		1584 vs		COO asymmetric stretch
1531 m,sh		1525 s		1523 s		
1430 vs	(1426 vs)[b]	1440 s		1421 s		COO symmetric stretch
	(1336 m)[b]	1312 w		1318 w,sh		CH_2 wagging
1282 w,m	1280 w,b	1281 vw				
	1223 m	1225 w		1226 w	1205 w	
1150 w	1168 w	1167 w	1170 w	1158 vw		CH_2 twisting
	1062 w	1070 w		1092 vw, sh		FeOH deformations
	1027 w					
				988 vw		CC stretch
945 w,b	948 w					
	889 w					
	815 w			796 w, str		CH_2 rocking
			761 s			
708 w	713 w					
		669 w,b			688 w	COO scissoring
			637 w	607 w,b	622 vw	COO wagging
562 w	(546 w) [b]		555 w		558 w	COO rocking
			526 m			
458 m	460 m			480 vw		Fe–OH stretch
399 s			403 w			Fe–O stretches
		395 m		385 m		
			387 w			
		359 w				
				347 w		
					340 vw	
325 m				324 w, sh		
316 m,sh	314 w					
	285 w		279 w			Skeletal deformations
228 m		227 m		223 m		
				206 m		
					185 vw, b	

[a]Band notations: b, broad; s, strong; vs, very strong; m, medium; w, weak; vw, very weak; sh, shoulder.

[b]Bands overlapping with the ligand modes.

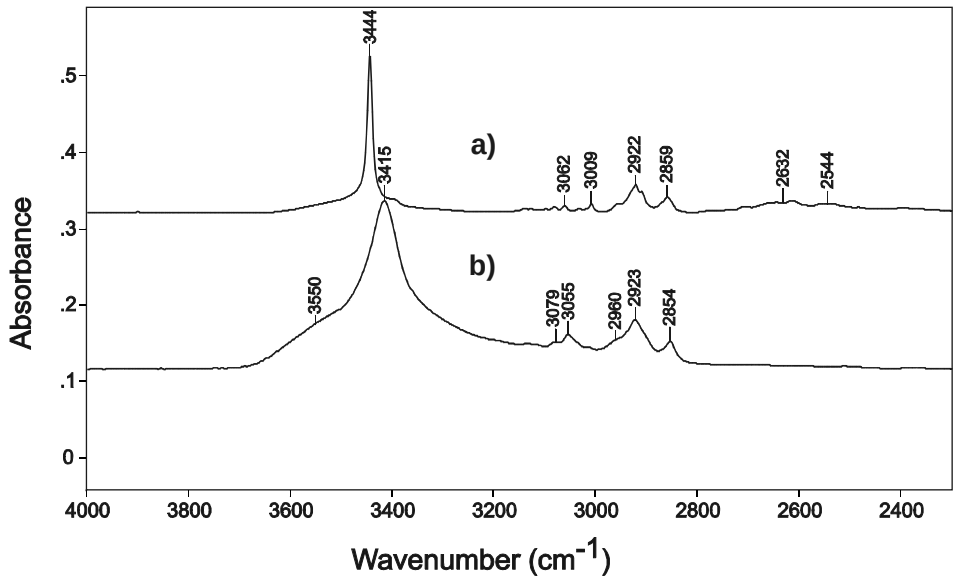

Fig. 6 Infrared spectra of free IPA (a) and the Fe–IPA complex (b) in the range of OH, NH and CH stretching regions

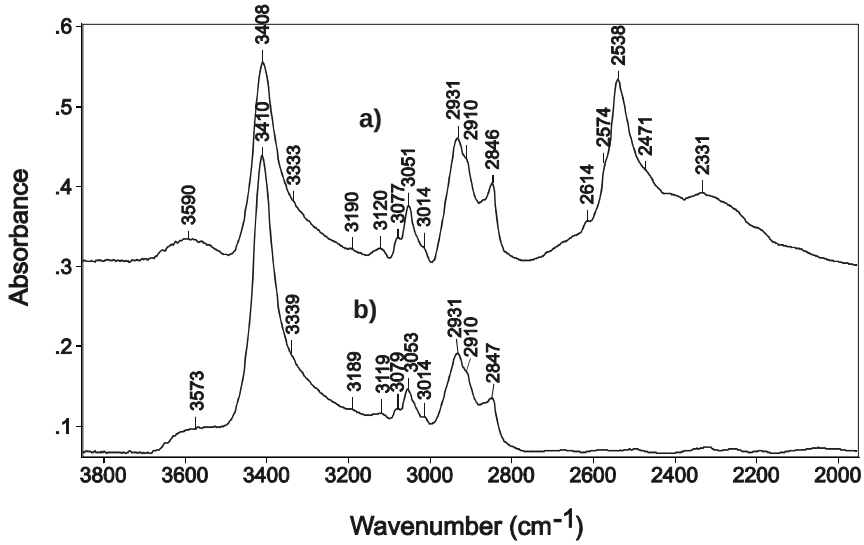

Fig. 7 Infrared spectra of the deuterated sample of the Fe–IBA complex (a) and the original nondeuterated sample (b)

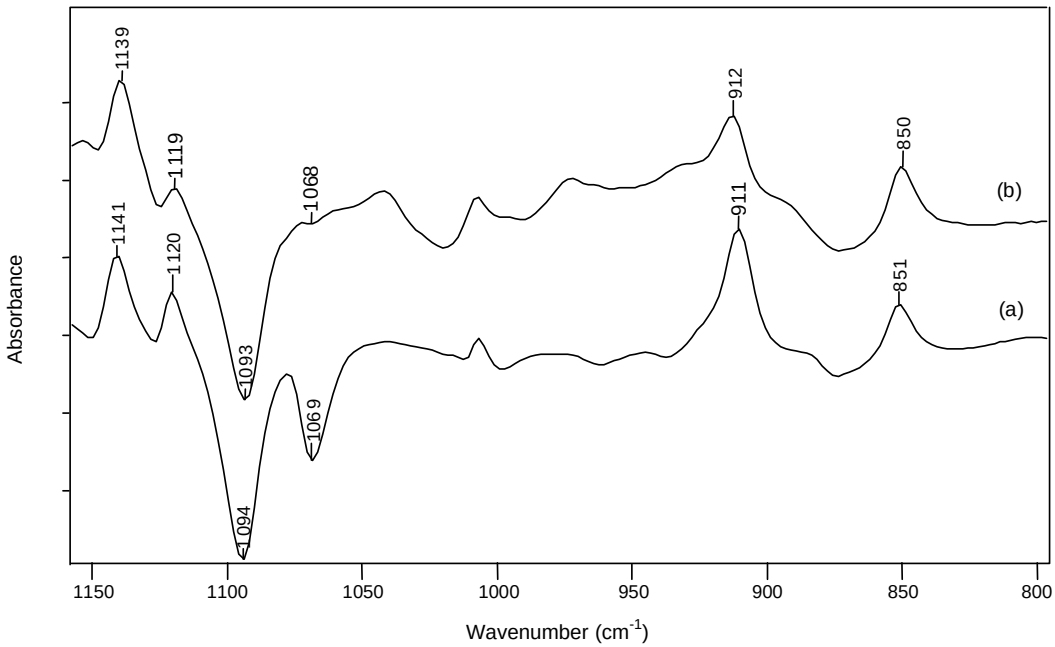

Fig. 8 Spectral difference between deuterated iron complexes (*upward bands*) and nondeuterated sample (*downward bands*) in the region of FeOH/FeOD deformational vibrations. (a) (Fe–IPA complex + D_2O vapour) − (Fe–IPA complex + H_2O vapour); (b) (Fe–IBA complex + D_2O vapour) − (Fe–IBA complex + H_2O vapour)

Infrared spectra of the Fe–IPA and Fe–IBA complexes in D_6-acetone were also recorded, and selected bands are presented in Table 8. Stretching frequencies of OH and NH groups were observed at almost the same positions as for the solid samples. Extra features, such as medium-intensity broad bands, were observed around 2520 and 2490 cm^{-1} characteristic of uncomplexed COOH groups. These bands had not been observed in the IR or Raman spectra of the solid complexes and can be attributed to the ligand exchange due to water traces, as discussed above.

Because of the strong overlap with the corresponding $(CD_3)_2CO$ absorption, the very strong C=O stretching mode of the –COOH group at 1700 cm^{-1} could not be observed. The existence of the –COOH group and the rather high frequency of the Fe–O stretching modes around 430 cm^{-1} (see Table 8) indicate that in solution the structure of the coordination sphere of iron in the complexes undergo some changes, as compared to that established for solid samples. These results are in agreement with the Mössbauer data (see above).

Table 7 Selected FTIR bands[a] of Fe–IPA and Fe–IBA complexes shifted due to D_2O exposure

Fe–IPA + H_2O[b]	Fe–IPA + D_2O[b]	Fe–IBA + H_2O[b]	Fe–IBA + D_2O[b]	Assignments	
3606 w	2693 vw	3613 w	2696 w	OH/OD stretch	
3552 w	2566 w, sh	3554 w	2613 w		
3412 s	2539 s	3410 s	2538 s	NH/ND stretch	
3340 m, b, sh	2471 w, sh	3331 m, b, sh	2489 m, b, sh	OH/OD stretches of strongly H-bonded groups or overtones of NH/ND deform	
	2415 w, b		2399 w, b, sh		
3117 w, b	2365 w, b	3114 w, b	2377 w, b 2260 w, sh		
1582 w [c]	1237 m	1581 w [c]	1237 m	NH/ND in-plane deformations	
1225 w	1141 w	1226 w	1139 w	CN stretch (ring)	
1094 w	911 w, m	1093 m	912 w, m	OH / OD in-plane deformations	
1069 w	851 w, m	1068 vw	850 w, m		
585 m	571 m	582 m	578 m	Fe, Fe >OH	OH out-of-plane deformations
471 w	446 m	480 m	473 m	Fe, Fe >OH	FeO stretch
228 w	210 vw, sh	233 vw	228 w	FeOFe deform	

[a]Band notations: b, broad; s, strong; vs, very strong; m, medium; w, weak; vw, very weak; sh, shoulder.

[b]All bands were obtained as the differences of [complex + H_2O(vapour)] – [complex + D_2O(vapour)].

[c]Strong overlapping with the H–O–H deformational band of adsorbed H_2O.

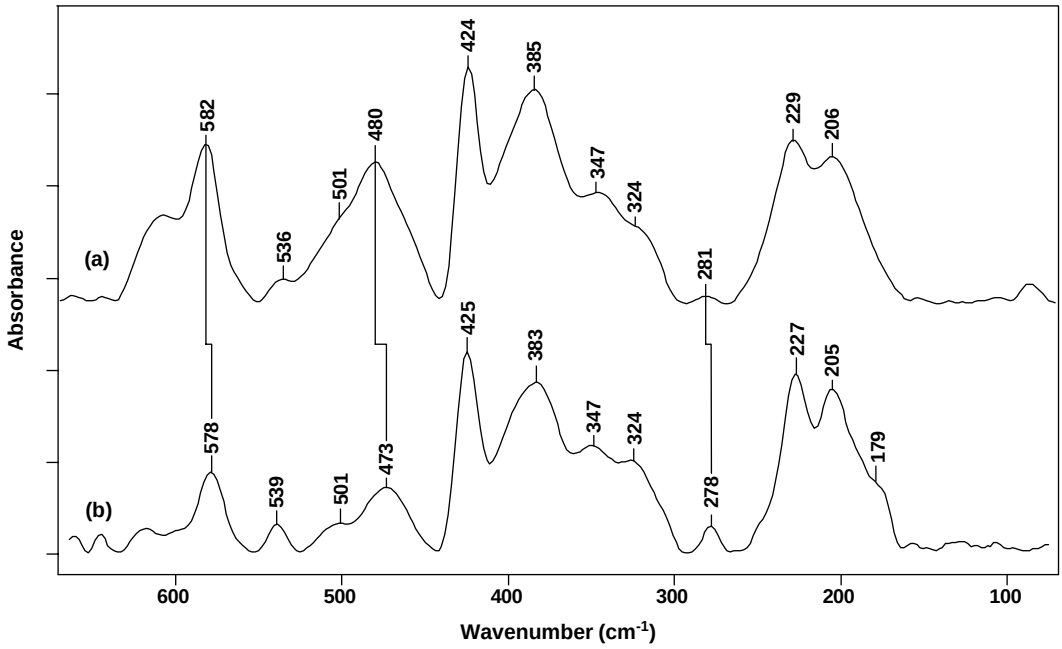

Fig. 9 Far-infrared spectra of the Fe–IBA complex (a) and the corresponding deuterated Fe–IBA sample (b). The strongest frequency shifts are marked with solid lines

Solution X-Ray diffraction study

Method of Structural Analysis

The observed structure functions $kh(k)$ and pair correlation functions $g(r)$ are shown in Fig. 12. As a first step, a visual evaluation and a preliminary semi-quantitative analysis was performed. Further on, the observed data were analysed by geometrical model constructions and fitting the model structure functions to the corresponding experimental ones by

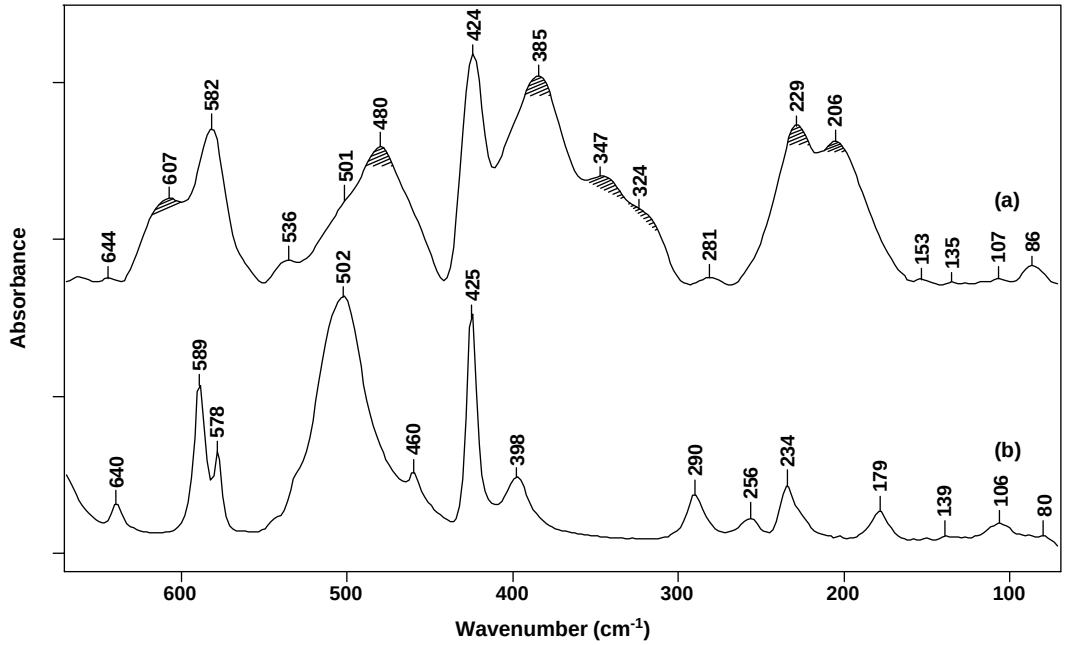

Fig. 10 Far-infrared spectra of the Fe–IBA complex (a) and free IBA (b). The new bands appearing in the complex are marked with shaded maxima

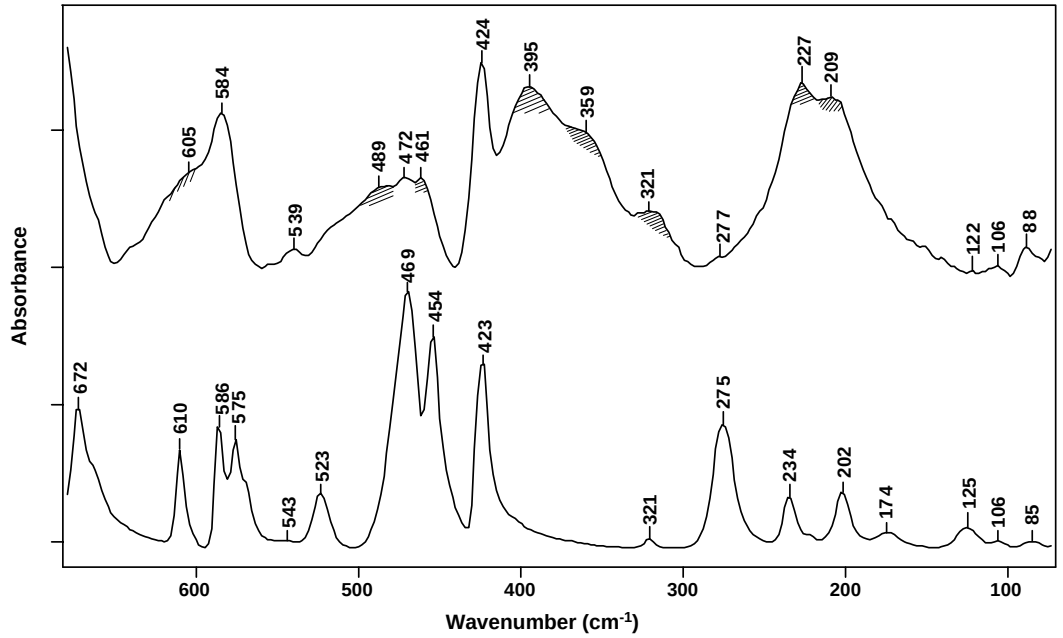

Fig. 11 Far-infrared spectra of the Fe–IPA complex (*upper spectrum*) and free IPA (*lower spectrum*). The new bands appearing in the complex are marked with shaded maxima

the non-linear least-squares method. The quality of fit was monitored through the S_{res} factor as

$$S_{\text{res}} = \sum_{k_{\min}}^{k_{\max}} k^2 [h(k)_{\text{exp}} - h(k)_{\text{calc}}]^2. \tag{3}$$

The theoretical intensities $h(k)_{\text{calc}}$ were calculated using the formulae

$$h_{\text{calc}}(k) = h_d(k) - h_c(k); \tag{4}$$

$$c_{\alpha\beta}(k) = \frac{(2 - \delta_{\alpha\beta}) x_\alpha x_\beta f_\alpha f_\beta}{M(k)}; \tag{5}$$

Table 8 Selected FTIR bands[a] of Fe–IPA and Fe–IBA complexes dissolved in D_6-acetone

Fe–IPA	Fe–IBA	Assignment
3591 m, b	3595 m	OH stretch
3545 m, b	3550 m, sh	
3415 m, sh	3415 m, sh	NH stretch
3392 vs	3379 vs	
3339 m, sh	3340 m, sh	
2617 w	2617 w, sh	Overtones and combinations of OH deformations and C–O stretches of –COOH group
2585 w	2578 w, sh	
2524 m	2523 m	
2493 m	2493 m	
2406 w, b	2412 w, sh	
891 w	892 w	C–C stretch and CH_2 rocking
884 w		
817 w, b	812 w, b	
598 w, b	615 w, b	COO rocking
427 m	426 m	Fe–O stretch
233 vw, b	233 vw, b	Skeletal def. (OFeO)

[a]Band notations: b, broad; s, strong; vs, very strong; m, medium; w, weak; vw, very weak; sh, shoulder.

$$h_d(k) = \sum_{\alpha\beta} c_{\alpha\beta}(k)\frac{n_{\alpha\beta}}{x_\beta}\frac{\sin(kr_{\alpha\beta})}{kr_{\alpha\beta}}\exp\left(-\frac{\sigma_{\alpha\beta}^2}{2}k^2\right); \quad (6)$$

$$h_c(k) = \sum_{\alpha\beta} 4\pi\rho_0 c_{\alpha\beta}(k)\frac{kR_{\alpha\beta}\cos(kR_{\alpha\beta}) - \sin(kR_{\alpha\beta})}{k^3} \exp\left(-\frac{\Gamma_{\alpha\beta}^2}{2}k^2\right), \quad (7)$$

where $c_{\alpha\beta}$ means k-dependent weights of different scattering contributions; α, β refer to scattering centres of different chemical types; $\delta_{\alpha\beta}$ is the Kronecker constant with values $\delta_{\alpha\beta} = 1$ if $\alpha = \beta$ and $\delta_{\alpha\beta} = 0$ if $\alpha \neq \beta$. The first term $h_d(k)$ (discrete part) represents the short-range interactions characterised by the interatomic distance $r_{\alpha\beta}$, the root mean square deviation $\sigma_{\alpha\beta}$ and the coordination number $n_{\alpha\beta}$. The second term $h_c(k)$ (continuum part) accounts for the uniform distribution of β type particles around α types beyond a given distance; $R_{\alpha\beta}$ and $\Gamma_{\alpha\beta}$ define the related boundary of the uniform distribution of α, β type distances and their root mean square deviation, respectively. Consequently, one contribution for each type of interaction was involved in $h_d(k)$ and $h_c(k)$ functions (Eqs. (6) and (7)), as shown in Table 9.

A visual inspection of the radial distribution functions indicated that they are rather composite, and no peaks, not even the main peak, can be uniquely assigned to a certain kind of interactions. The first peak is centred around 1.45 Å, the second one around 2 Å. As can be seen in Fig. 13, more than one interaction gives rise to these peaks. In order to give a quantitative description of the structure (i.e., to derive the structural parameters, the coordination numbers, mean interatomic distances and their root mean square deviations, at least for the contributions of the predominant interactions), the construction and fitting of extensive structural models were necessary.

Table 9 Structural parameters for $[Fe_2(OH)_2(IA)_4]$ (where IA is indole-3-acetate) dissolved in methanol (with the estimated errors in the last digits)

Complex Bond	*r* (Å)	*n*	*l*
Fe–O	2.00 (0.01)	5 (0.01)	0.10
Fe–Fe	3.01 (0.01)	1 (0.01)	0.20
Fe–C1	2.9 (0.02)	2 (0.05)	0.2
Fe–C2	3.96 (0.05)	3.8 (0.5)	0.25
Fe–C3	4.64 (0.05)	3.4 (0.5)	0.35
Fe–C4	5.00	6	0.35
O–O[a]	2.50 (0.03)	1 (0.02)	0.10
O–O[b]	2.83 (0.02)	2.8 (0.05)	0.10
C–C1	4.75	2	0.25
C–C2	5.20	2	0.30
Solvent			
O–O	2.85 (0.05)	1.6 (0.5)	0.17
C–O	3.46 (0.05)	2.8 (0.5)	0.25
C–C	4.61(0.05)	4.6 (0.5)	0.40
Complex–solvent			
C–O	3.58 (0.08)	2	0.30

The distances (r) and the mean square deviations (σ) are given in Å. Parameters without estimated errors were derived from the model and kept constant.

[a]Hydroxo-bridge.

[b]Around Fe atom.

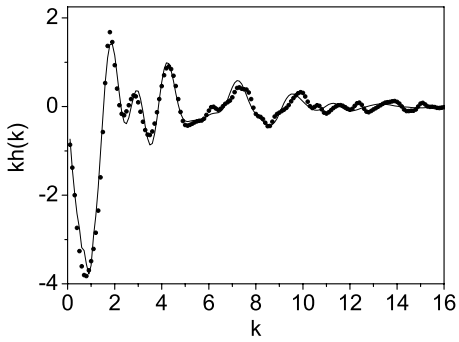

Fig. 12 Structure functions $h(k)$ multiplied by k for $[Fe_2(OH)_2(IA)_4]$ (where IA represents indole-3-acetate) in methanol solution. The experimental values are given by points, and the theoretical values by *solid lines*

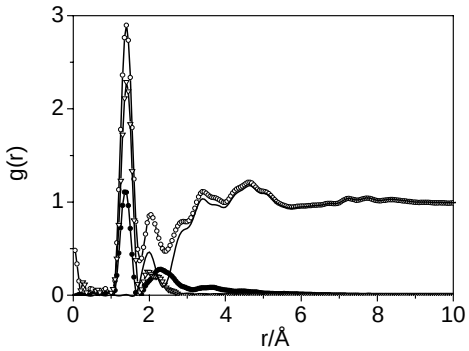

Fig. 13 Pair correlation functions $g(r)$ and intramolecular contributions for $[Fe_2(OH)_2(IA)_4]$ (where IA represents indole-3-acetate) in methanol solution. *Open circles*: total pair correlation function; *circles*: intramolecular contribution from the ligand; *open downward triangles*: intramolecular contribution from the solvent; *solid line*: difference pair correlation

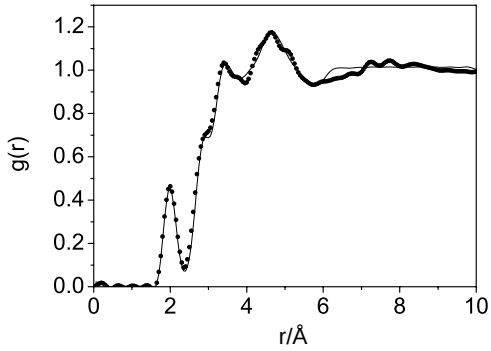

Fig. 14 Difference pair correlation functions $g(r)$ and intramolecular contributions for $[Fe_2(OH)_2(IA)_4]$ (where IA represents indole-3-acetate) in methanol solution. *Points*: experimental values; *solid line*: theoretical (fitted) values

The fitting strategy was the following. At the beginning, the "rough" structure of the complex was fixed by inputting the structural parameters obtained from the preliminary single-crystal study of the ligand [27]. The parameters of the discrete structure were kept constant and those for the continuum were adjusted. Then the complex–solvent and solvent–solvent interactions were included in the fitting procedure. The refinement extended over the k range $0.2 \leq k \leq 15.3$ Å^{-1}. In the next step, all coordination numbers were kept constant, whereas distances and root mean square deviations were adjusted. Next, most of the coordination numbers were allowed to vary. This process was repeated alternately several times until the minimum S_{res} factor had been reached. Finally an overall check was run, letting all parameters vary, covering the entire k range. As can be seen, the data evaluation procedure did not comprise any geometrical constraint between the distance parameters computed by any assumed regular symmetry. The models suggested were built up on the basis of parameters obtained from the fitting procedure.

Results of the solution X-Ray diffraction measurements

As mentioned above, the experimental and theoretical X-ray structure functions obtained are shown in Fig. 12; the $g(r)$ functions are shown in Figs. 13 and 14.

The following intramolecular contributions give rise to the first peak centred around 1.45 Å: intramolecular contributions from methanol, C–O, C–H, O–H; from the ligand, C–O, C–N, C–H, O–H. All these intramolecular interactions are shown in Fig. 13. These interactions contribute obviously to the next peak, at 2 Å, too. After subtracting the above intramolecular contributions from the total partial correlation function of the solution, the difference partial correlation function was obtained, as shown in Fig. 14. With this operation, the evaluation of the peak at 2 Å becomes more obvious. For this peak, the Fe–O interaction is responsible. A shoulder can be observed at 2.9 Å; there appear the O–O interactions from the solvent and the complex, further on the Fe–C and Fe–Fe interactions. A rather complex main peak can be observed around 3.5 Å. This peak can be assigned to two types of C–O interactions, first between the methanol molecules, second between the carbon atom of the complex and oxygen atom of the surrounding methanol molecules. Another broad peak appears in the range 4–6 Å. Carbon–carbon interactions from the complex and from the solvation shell around the complex are responsible for these peaks, which are difficult to resolve because of their complexity, and therefore a model analysis can only tentatively reveal the major contributions to them.

The structural parameters, obtained from the least-squares fit of the structure functions $kh(k)$ shown in Fig. 12, are given in Table 9. An examination of the weights of the contributions to the structure function shows that the ion–ion type interactions are negligible compared to the others.

Accordingly, in $h_d(k)$ and $h_c(k)$ functions (Eqs. (6) and (7)) only one contribution for each type of interaction, listed in Table 9, was included. The fitting procedure resulted in 2.00 ± 0.01 Å for the Fe–O distance. The Fe–Fe distance was found to be 3.01 Å. The average Fe–O coordination number is 5 ± 0.01; O–O, corresponding to the hydroxo-bridge and Fe–Fe coordination numbers are 1. These data can be interpreted with a structure represented in Fig. 15. Each iron atom is surrounded by six oxygen atoms as follows: four from two deprotonated IAA ligands and two from the dihydroxo-bridge linking the two iron atoms. This configuration is also supported by the values of distances found for the O–O interaction around the iron atom (2.83 Å), Fe–C and C–C interactions obtained.

The O–O interaction in the solvent gives the value around 2.85 Å, while the O–O coordination number sums up to

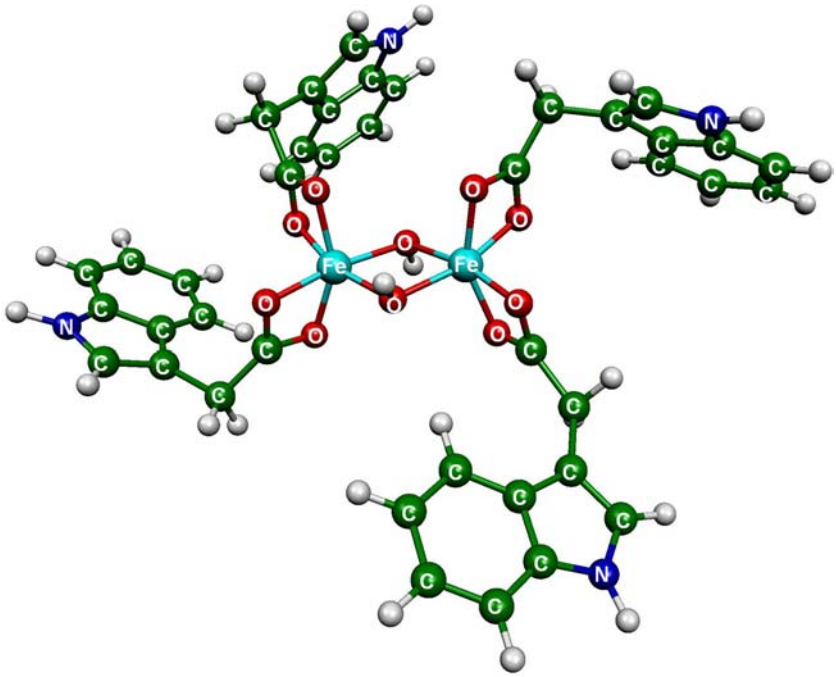

Fig. 15 Schematic ball-and-stick representation of the $[Fe_2(OH)_2(IA)_4]$ complex (IA represents indole-3-acetate)

1.6 ± 0.5. For comparison, it is worth noting that in pure liquid methanol the corresponding O–O distance was reported [28] to be around 2.80 Å and the coordination number about 1.8. The complex is surrounded by methanol molecules, thus forming an additional second shell around the central iron ions. About two methanol molecules are located at a distance of 3.58 Å from each carbon atom of the ligand.

Acknowledgements The authors are grateful to Professor G. Pálinkás (Budapest, Hungary), Dr. P. A. Tarantilis (Athens, Greece) and Dr. A. G. Shchelochkov (Saratov, Russia) for many stimulating discussions and to L. Hajba for recording the far-infrared spectra.

This work was supported in parts by The Hungarian Science Foundation (OTKA Grant T43687), NATO (Expert Visit Grants LST.EV.980141 and CBP.NR.NREV.981748; Collaborative Linkage Grants LST.CLG.977664 and LST.NR.CLG.981092), Russian Academy of Sciences' Commission (Grant No. 205 under the 6th Competition-Expertise of research projects), as well as under the Agreements on Scientific Cooperation between the Russian and Hungarian Academies of Sciences for 2002–2004 and 2005–2007.

References

1. Marumo S (1986) In: Takahashi N (ed) Chemistry of plant hormones. CRC Press, Inc., Boca Raton, Florida (USA), Chapter 2, pp 9–56
2. Weyers JDB, Paterson NW (2001) New Phytologist 152:375–407
3. Woodward AW, Bartel B (2005) Ann Bot (London) 95:707–735
4. Lambrecht M, Okon Y, Vande Broek A, Vanderleyden J (2000) Trends Microbiol 8:298–300
5. Costacurta A, Vanderleyden J (1995) Crit Rev Microbiol 21:1–18
6. Kamnev AA, Kuzmann E (1997) Biochem Mol Biol Int 41:575–581
7. Kamnev AA, Kuzmann E (1997) In: Carmona P, Navarro R, Hernanz A, (eds) Spectroscopy of biological molecules: Modern trends. Annex. UNED Press, Madrid, pp 85–86
8. Kamnev AA, Shchelochkov AG, Perfiliev YuD, Tarantilis PA, Polissiou MG (2001) J Mol Struct 563–564, 565–572
9. Kamnev AA, Kuzmann E, Perfiliev YuD, Vankó Gy, Vértes A (1999) J Mol Struct 482–483, 703–711
10. Kovács K, Kamnev AA, Shchelochkov AG, Kuzmann E, Medzihradszky-Schweiger H, Mink J, Vértes A (2004) J Radioanal Nucl Chem 262:151–156
11. Kamnev AA, Kuzmann E, Perfiliev YuD, Vértes A, Ristić M, Popović S, Musić S (2000) J Radioanal Nucl Chem 246:123–129
12. Gazaryan IG, Lagrimini LM, Ashby GA, Thorneley RNF (1996) Biochem J 313:841–847
13. Hinman RL, Lang J (1965) Biochemistry (USA) 4:144–158
14. Harrod JF, Guerin C (1979) Inorg Chim Acta 37:141–144
15. Vértes A, Parak F (1971) J Chem Soc Dalton Trans 2062–2068
16. Klencsár Z, Kuzmann E, Vértes A (1996) J Radioanal Nucl Chem 210:105–114
17. Radnai T, Ohtaki H (1996) Mol Phys 87:103–121
18. Hajdu F, Pálinkás G (1972) J Appl Cryst 5:395–401
19. Levy HA, Danford MD, Narten AH (1966) Oak Ridge National Laboratory Rep., Nr. 3960, 54 pp
20. Hajdu F (1972) Acta Cryst A28:250–252
21. Pálinkás G, Radnai T (1976) Acta Cryst A32:666–668
22. Krogh-Moe K (1956) Acta Cryst 2:951–953
23. Cromer DT, Waber JT (1965) Acta Cryst 18:104–109
24. International Tables for X-ray Crystallography (1974) vol 4, The Kynoch Press, Birmingham (UK), pp 366
25. Vértes A, Nagy DL (eds) (1990) Mössbauer spectroscopy of frozen solutions, Akad Kiadó, Budapest
26. Ferraro JR, Walker WR (1965) Inorg. Chem, 4:1382–1386
27. Degen A, Bolte M (2001) Acta Cryst. E – Structure Reports Online, 57, Part 11, O999-O1000
28. Narten AH, Habenschuss A (1984) J Chem Phys 80:3387–3391